BIOCHEMISTRY
including biophysical chemistry & molecular biology
Article

Biochemistry **2010,** *49,* 1331–1337 1331
DOI: 10.1021/bi901810u

Eribulin Binds at Microtubule Ends to a Single Site on Tubulin To Suppress Dynamic Instability†

Jennifer A. Smith,‡ Leslie Wilson,‡ Olga Azarenko,‡ Xiaojie Zhu,§ Bryan M. Lewis,§ Bruce A. Littlefield,∥,⊥ and Mary Ann Jordan*,‡

‡*Department of Molecular, Cellular, and Developmental Biology and Neuroscience Research Institute, University of California, Santa Barbara, California 93106,* §*Process Development, and* ∥*Scientific Administration, Eisai Research Institute, Andover, Massachusetts 01810.* ⊥*Current address: Harvard Medical School, Landmark 22A-West, 401 Park Dr., Boston, MA 01810.*

Received October 22, 2009; Revised Manuscript Received December 21, 2009

ABSTRACT: Eribulin mesylate (E7389), a synthetic analogue of the marine natural product halichondrin B, is in phase III clinical trials for the treatment of cancer. Eribulin targets microtubules, suppressing dynamic instability at microtubule plus ends through an inhibition of microtubule growth with little or no effect on shortening [Jordan, M. A., et al. (2005) *Mol. Cancer Ther. 4*, 1086−1095]. Using [^{3}H]eribulin, we found that eribulin binds soluble tubulin at a single site; however, this binding is complex with an overall K_d of 46 μM, but also showing a real or apparent very high affinity (K_d = 0.4 μM) for a subset of 25% of the tubulin. Eribulin also binds microtubules with a maximum stoichiometry of 14.7 ± 1.3 molecules per microtubule (K_d = 3.5 μM), strongly suggesting the presence of a relatively high-affinity binding site at microtubule ends. At 100 nM, the concentration that inhibits microtubule plus end growth by 50%, we found that one molecule of eribulin is bound per two microtubules, indicating that the binding of a single eribulin molecule at a microtubule end can potently inhibit its growth. Eribulin does not suppress dynamic instability at microtubule minus ends. Preincubation of microtubules with 2 or 4 μM vinblastine induced additional lower-affinity eribulin binding sites, most likely at splayed microtubule ends. Overall, our results indicate that eribulin binds with high affinity to microtubule plus ends and thereby suppresses dynamic instability.

Eribulin mesylate is a tubulin- and microtubule-targeting chemotherapeutic drug that inhibits the proliferation of multiple cancer cell types (*1*, *2*). It is a synthetic analogue of the natural compound halichondrin B (Figure 1A), initially isolated from the sea sponge *Halichondria okadai* (*3*). Eribulin is currently in phase III clinical trials for the treatment of metastatic breast cancer. Phase I and phase II clinical trials have demonstrated that eribulin is active in heavily pretreated individuals while maintaining a tolerable therapeutic index, with the most frequent adverse effects being neutropenia and fatigue (*4*−*6*). Neuropathy, a common dose-limiting toxicity of other microtubule-targeting drugs like paclitaxel and some vinca alkaloids (*7*−*9*), has a low incidence in eribulin-treated patients, and no grade 4 neuropathy occurred (*4*−*6*).

Eribulin exerts its anticancer properties through a novel action on tubulin and microtubules (*1*, *10*−*12*). In MCF7 cells, eribulin inhibited microtubule dynamic instability at low concentrations and induced depolymerization of the microtubule network at high concentrations (10 × IC_{50} for inhibition of cell proliferation) (*11*). At significantly lower eribulin concentrations, eribulin potently inhibited microtubule dynamics, resulting in prolonged mitotic arrest and subsequent apoptosis (for a review of microtubule structure and dynamic instability, see refs *13* and *14*). Eribulin binds at or near the vinca domain, a region that is located at the interface of two tubulin heterodimers when arranged end to end and overlaps the exchangeable GTP[1] site on β-tubulin (*2*, *10*, *15*−*17*). Eribulin inhibits binding of vinblastine to free tubulin noncompetitively with an apparent K_i of 1.9 μM, and it inhibits GTP hydrolysis and exchange (*2*), as do most compounds that bind in the vinca domain (*16*).

Microtubules undergo complex growth and shortening events, termed dynamic instability. Microtubule-targeting drugs inhibit dynamic instability by altering tubulin addition and loss parameters, which in turn inhibits the ability of a cell to undergo successful mitotic division (*14*). Eribulin's effects on dynamic instability are novel, in that eribulin suppresses the growth parameters at microtubule plus ends without affecting microtubule shortening parameters, both in cells and in a purified in vitro system (*11*), resulting in an overall decrease in dynamicity. On the basis of these findings, we hypothesized that eribulin preferentially binds tubulin at microtubule ends, thus blocking the addition of tubulin dimers to a growing end.

To determine the mechanism by which eribulin suppresses microtubule growth, we examined the binding of eribulin to soluble tubulin and to polymerized microtubules using radiolabeled eribulin. We also examined the effects of eribulin on steady-state microtubule polymer mass and on the dynamic

†Supported by grants from Eisai Research Institute and National Institutes of Health Grants CA 57291 and NS13560.

*To whom correspondence should be addressed: Molecular, Cellular, and Developmental Biology, University of California, Santa Barbara, CA 93106. Phone: (805) 893-5317. Fax: (805) 893-5081. E-mail: jordan@lifesci.ucsb.edu.

[1]Abbreviations: DMSO, dimethyl sulfoxide; EGTA, ethylene glycol tetraacetic acid; GTP, guanosine 5′-triphosphate; MAP, microtubule-associated protein; MES, 2-(*N*-morpholino)ethanesulfonic acid; PIPES, 1,4-piperazine bis(2-ethanosulfonic acid); SEM, standard error of the mean.

Published on Web 12/23/2009

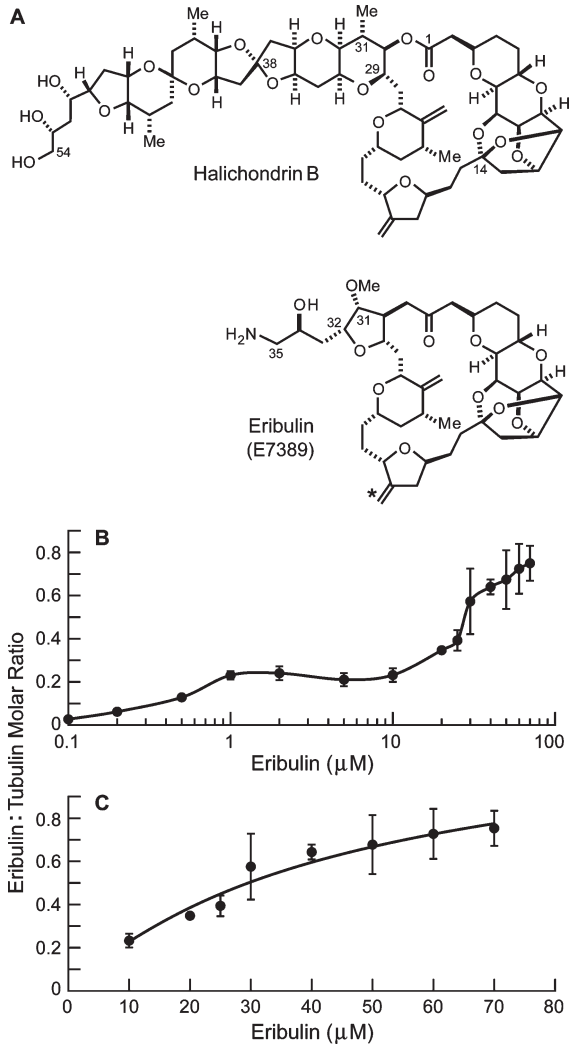

FIGURE 1: (A) Eribulin (E7389) and its parent compound, halichondrin B. The location of tritiation in [^{3}H]eribulin is indicated with an asterisk. (B) Binding of eribulin to soluble tubulin. (C) Enlargement of panel B showing the binding of eribulin to soluble tubulin with the curve determined by nonlinear regression. [^{3}H]Eribulin was incubated with soluble MAP-depleted bovine brain tubulin (2 μM) for 20 min at 30 °C, followed by centrifugation through a microspin gel filtration column. Data are means ± SEM of three to six experiments.

instability of minus ends. Our results indicate that eribulin binds to a single site on tubulin heterodimers and that eribulin binds to microtubule ends, most likely at plus ends. We found that binding of vinblastine to microtubules inhibited eribulin binding at low eribulin concentrations but also appeared to open additional, low-affinity binding locations for eribulin, at either one or both microtubule ends.

MATERIALS AND METHODS

Eribulin. Eribulin (NSC-707389; previously E7389, ER-086526) and tritium-labeled eribulin (specific activity of 2.3 × 10^4 Ci/mol) were synthesized at Eisai Research Institute (*18*).

Purification of Microtubule Protein and Tubulin. Bovine brain microtubule protein consisting of approximately 70% tubulin and 30% microtubule-associated proteins (MAPs) was purified without glycerol by three cycles of polymerization and depolymerization; tubulin was purified from the microtubule protein by phosphocellulose chromatography and stored at −70 °C as previously described (*19*). Immediately before each experiment, tubulin was thawed and cleared of aggregated protein by centrifugation at 66000*g* for 30 min (4 °C). The protein concentration in all experiments was determined by a Bradford assay with bovine serum albumin as the standard (*20*).

Eribulin Binding to Soluble Tubulin. Phosphocellulose-purified tubulin (1.8 μM) in PEM 50 buffer [50 mM PIPES, 1 mM EGTA, and 1 mM $MgSO_4$ (pH 6.9)] and 100 μM GTP was incubated with [^{3}H]eribulin (0.1−70 μM) for 20 min at room temperature (22 °C), and then 100 μL of each sample was added to a Zeba microspin desalting column (Thermo Fisher Scientific, Inc., Waltham, MA). The specific activity of each sample was measured immediately after addition of eribulin. Columns were centrifuged for 2 min at 1500*g* following the manufacturer's instructions. The protein content and radioactivity in the tubulin flow-through were determined. Background radiolabel was assessed by centrifuging samples without protein at the concentrations of eribulin used. Background radioactivity levels correlated with the eribulin concentration, with an average of 4.2% of the starting eribulin passing through the column with no protein present. This value was subtracted from all experimental radioactivity measurements.

Equilibrium binding data were quantified by measuring the fraction of tubulin bound with eribulin at various eribulin concentrations and a single fixed concentration of tubulin (2 μM). The following model for simple hyperbolic binding was fit to the data:

$$Y_D = Y_{max} D/(K_d + D)$$

In this model, D is the total concentration of eribulin, Y_D and Y_{max} are the ratios of bound eribulin to tubulin at subsaturating and infinite concentrations of D, respectively, and K_d is the equilibrium binding constant. The best-fit values for Y_{max} and K_d were determined by nonlinear regression using KaleidaGraph version 3.5 (Synergy Software, Reading, PA). Y_{max} and K_d values and standard errors of binding of eribulin to soluble tubulin were calculated using all data points as a single data set.

Microtubule Depolymerization. Microtubule depolymerization was measured by turbidity using a temperature-controlled Beckman Coulter (Fullerton, CA) spectrophotometer. Polymerization of MAP-rich tubulin (3 mg/mL) was initiated by incubation at 30 °C for 30 min in PEM 100 buffer [100 mM PIPES, 1 mM EGTA, and 1 mM $MgSO_4$ (pH 6.9)] and 1 mM GTP. Microtubules were then sheared eight times through a 25 gauge needle and allowed to regain steady state for 15 min. Aliquots of a microtubule suspension (100 μL) were added to cuvettes and placed in a warmed spectrophotometer at 30 °C. Eribulin (1−20 μM) was added at time zero, and absorbance readings were taken at a wavelength of 350 nm every minute for 30 min.

Dynamic Instability of Microtubule Minus Ends. The dynamic instability of microtubules in the presence of eribulin was measured as described previously (*19*, *21*, *22*). Briefly, microtubules (18 μM tubulin) were assembled from phosphocellulose-purified tubulin in PMEM buffer [86 mM PIPES, 26 mM MES, 1 mM EGTA, and 1.4 mM $MgSO_4$ (pH 6.8)] and 1 mM GTP in the presence or absence of eribulin. Microtubules were nucleated using sea urchin flagellar axonemal fragments and incubated at 35 °C for 30 min to achieve steady state. The behavior of individual microtubules was recorded by video-enhanced differential interference contrast microscopy with an IX71 Olympus (Melville, NY) inverted microscope and analyzed for growth and shortening events. Minus ends were distinguished from plus ends as described previously (*23*).

Between 45 and 50 growth and shortening events were measured for each condition.

Eribulin Binding to Microtubules and Microtubule Length Determination. Microtubules were assembled from MAP-rich tubulin (3 mg/mL) and sheared to obtain a large number of short microtubules as described above and then incubated for an additional 20 min to regain steady state. [^{3}H]Eribulin was added (0.1−10 μM) to 375 μL of sheared microtubules, and samples were immediately layered onto a microtubule stabilizing cushion (30% glycerol and 10% DMSO in PEM buffer) to minimize depolymerization at high eribulin concentrations (the incubation time with drug was approximately 1−2 min). Microtubules were collected by centrifugation in an SW 50.1 swinging bucket rotor using a Beckman Coulter Optima ultracentrifuge (108000*g* for 60 min at 30 °C). The soluble fraction was discarded, and microtubule pellets were carefully washed with PEM buffer and dissolved in 0.1 N NaOH at 4 °C overnight. The protein content and radioactivity of pellets were measured the following day. Background radiolabel was measured by performing parallel assays using 20 μM podophyllotoxin to inhibit microtubule polymerization (*24*). All results are reported with the background subtracted.

Microtubule lengths were determined by electron microscopy for use in determination of the stoichiometry of binding of eribulin to microtubules. Lengths of a minimum of 300 microtubules were measured for each experiment. For controls, the mean microtubule length ranged from 2.4 to 4.2 μm per experiment, with an overall mean of ~3 μm. Microtubules, either without eribulin addition for controls or after eribulin incubation as described below, were fixed with 0.2% glutaraldehyde, placed on electron microscopy grids, stained with cytochrome *c* (1 mg/mL) and 1% uranyl acetate, and imaged using a JEOL 1230 transmission electron microscope (80 kV) (*11*).

To account for eribulin-induced changes in microtubule length in the determination of stoichiometry, microtubules were incubated with the stated eribulin concentrations for 1−2 min and centrifuged through a DMSO/glycerol stabilizing cushion into a denser layer of 70% sucrose. Pelleted microtubules were fixed and stained as described above and their lengths measured by electron microscopy. At concentrations of 5 and 10 μM, eribulin reduced the mean microtubule length by 17 and 29%, respectively. These length changes were factored into the calculations of bound eribulin per microtubule for these two concentrations.

The number of eribulin molecules bound per microtubule was calculated using the mass and radioactivity of each pellet, the mean measured value for microtubule length, and the factor of 1690 tubulin heterodimers per micrometer (*25*). The number of microtubules per liter was calculated for each sample using the microtubule pellet mass for that sample. Nonlinear regression of binding data was computed using KaleidaGraph version 3.5 (Synergy Software) using the equation given above. Y_{max} (ratio of bound eribulin molecules per microtubule) and K_d values for binding of eribulin to microtubules were calculated for individual experiments, and the mean and standard error for all experiments were determined.

Effects of Vinblastine on Binding of Eribulin to Microtubules. Unlabeled vinblastine (Sigma, St. Louis, MO) was added to sheared MAP-rich microtubules at a concentration of 2 or 4 μM for 15 min before [^{3}H]eribulin was added, and then samples were treated as described above. Electron microscopy samples for length measurements were taken after vinblastine incubation, but before eribulin addition. Consistent with previous findings that vinblastine stabilizes microtubule ends against shortening (*11*, *19*, *26*), in the presence of vinblastine (2 or 4 μM), eribulin induced no significant changes in microtubule length; therefore, the stoichiometry of eribulin bound per microtubule in the presence of vinblastine was calculated using the vinblastine-treated microtubule length measured in each experiment.

Morphology of Microtubule Ends. To determine the effects of the drug on microtubule ends, unsheared microtubules were incubated with no drug, 50 μM eribulin, or 50 μM vinblastine for 15 min, and then 5 μL of sample was gently added to 15 μL of glutaraldehyde (final concentration of 0.1%) on an electron microscope grid and stained as described above. Both ends of 50 microtubules each for control and eribulin-treated microtubules and 30 microtubules for vinblastine-treated microtubules were examined and categorized as blunt, slightly splayed, or extensively splayed and/or spiraled.

RESULTS

Eribulin Binds a Single Site on α/β-Tubulin Heterodimers. We measured the stoichiometry of binding of [^{3}H]eribulin to soluble bovine brain tubulin using centrifugal gel filtration. [^{3}H]Eribulin was incubated with tubulin (2 μM for 20 min at 30 °C); then bound and free drug were separated by centrifugation using a microspin gel column (Materials and Methods), and the stoichiometry of eribulin bound to tubulin was determined. The binding curve is complex (shown on a logarithmic scale in Figure 1B). To simplify the interpretation, we analyzed eribulin binding for concentrations of ≤10 and ≥10 μM as two separate data sets. At low concentrations (0.1−10 μM), binding reached a plateau when approximately 25% of the tubulin was bound, with a Y_{max} of 0.26 ± 0.02 and a K_d of 0.4 ± 0.2 μM (determined by fitting the points for ≤10 μM eribulin to the hyperbolic binding equation presented in Materials and Methods). Between 10 and 30 μM eribulin, the level of binding increased sharply and approached saturation, as indicated by the change in the slope of the curve. At 70 μM, the stoichiometry was 0.8 eribulin molecule per tubulin dimer. At concentrations of > 70 μM, data were highly scattered (not shown), likely due to a high background. Overall, eribulin bound soluble tubulin with a Y_{max} of 1.3 ± 0.4 eribulin molecules per heterodimer and a K_d of 46 ± 28 μM eribulin (determined by fitting the points for ≥10 μM eribulin to the equation in Materials and Methods) (Figure 1C).

Eribulin-Induced Depolymerization of Microtubules. Eribulin (1−20 μM) was added to steady-state MAP-rich microtubules, and changes in microtubule polymer mass were examined by turbidity for 30 min (Figure 2A). Microtubules underwent an immediate, but partial, depolymerization in the first minute. By 30 min, microtubule polymer mass had relaxed to a new steady state. The final extent of depolymerization increased in a linear, concentration-dependent manner (Figure 2B) (R^2 = 0.96). At 30 min, there was a 4.5% decrease in polymer mass at 1 μM eribulin and an 80% decrease at 20 μM eribulin. A 50% reduction in polymer mass occurred at 11 μM eribulin.

Eribulin Does Not Affect Dynamic Instability at Microtubule Minus Ends. Previous results indicated that eribulin inhibits dynamic instability at microtubule plus ends (*11*), but the effects on minus ends had not been determined. Microtubules were assembled at 35 °C using sea urchin axoneme nucleating seeds and recorded for 10 min by video-enhanced differential interference contrast microscopy, and the dynamic instability at

Table 1: Plus and Minus End Microtubule Dynamic Instability in the Presence of 100 nM Eribulin

	plus end[a]			minus end		
	control	eribulin, 100 nM	percent change	control	eribulin, 100 nM	percent change
growth rate (μm/min)	0.9 ± 0.1[b]	0.5 ± 0.04	−46[c]	0.6 ± 0.1	0.6 ± 0.02	ns[e]
growing length (μm)	2.4 ± 0.3	1.2 ± 0.2	−50	0.9 ± 0.1	0.8 ± 0.1	ns[e]
shortening rate (μm/min)	33 ± 1.9	24 ± 1.9	[d]	14 ± 1.7	18 ± 3.7	ns[e]
shortening length (μm)	5.9 ± 0.5	3.7 ± 0.4	[d]	2.7 ± 0.4	3.5 ± 0.2	ns[e]
time growing (%)	85	74		28	25	
time shortening (%)	5	5		9	11	
time attenuated (%)	10	21		63	64	
catastrophe frequency per minute	0.3	0.3	ns[e]	0.2	0.4	ns[e]
rescue frequency per minute	2.4	2.2	ns[e]	2.3	1.9	ns[e]
dynamicity	2.4	1.4	−40	0.4	0.5	

[a]Plus end data were previously reported by Jordan et al. (*11*). [b]Value ± SEM. [c]Values were considered significant from controls at the 99% confidence level by a Student's *t* test. [d]Shortening rates in the presence of drug were not considered reliable because of the artificially reduced shortening lengths due to the shorter overall lengths of the microtubules. [e]Not significant.

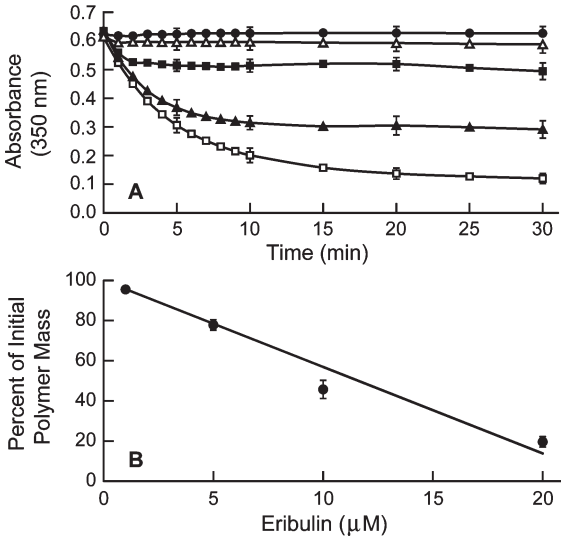

FIGURE 2: Eribulin-induced depolymerization of MAP-rich microtubules. (A) Control (●) and 1 (△), 5 (■), 10 (▲), and 20 μM eribulin (□). (B) Extent of final depolymerization 30 min after addition of eribulin. MAP-rich tubulin (3 mg/mL) was assembled to steady state; eribulin was added at time zero, and depolymerization was followed by turbidity (A_{350}). Data are means ± SEM of four to five experiments.

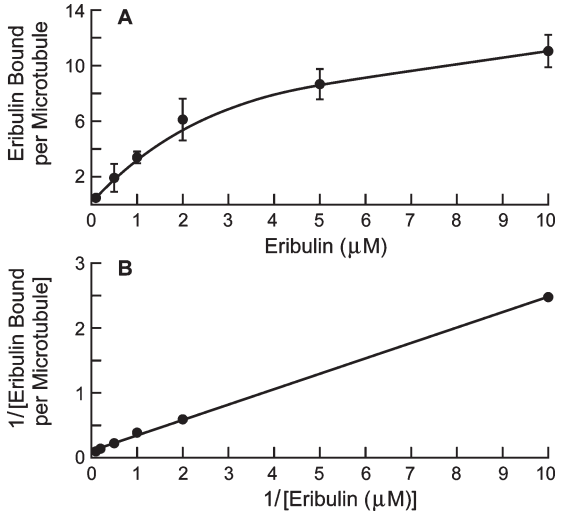

FIGURE 3: Binding of eribulin to microtubules. (A) Eribulin binds microtubules at a maximum of ~15 molecules per microtubule. (B) Double-reciprocal plot of binding of eribulin to microtubules of a representative experiment (R^2 = 0.99). MAP-rich tubulin (3 mg/mL) was assembled to steady state and then incubated with [^{3}H]eribulin for 1−2 min, followed by centrifugation through a stabilizing cushion. Data are means ± SEM of four experiments.

microtubule minus ends was analyzed (Materials and Methods). As listed in Table 1, in the absence of eribulin, minus ends of microtubules were less dynamic than plus ends. In contrast to the eribulin-induced suppression of growth rates and lengths at plus ends (46 and 50%, respectively), 100 nM eribulin had no significant effect on any parameters of dynamic instability at minus ends.

Eribulin Binds to Microtubule Ends at a Maximum Stoichiometry of ~15 Eribulin Molecules per Microtubule. To examine the binding of eribulin to microtubules, MAP-rich microtubules were polymerized to steady state, sheared to increase the number of microtubule ends, incubated with [^{3}H]eribulin (0.1−10 μM) for 1−2 min, and collected by centrifugation through a glycerol/DMSO stabilizing cushion.

By calculating the eribulin bound per microtubule using the eribulin and tubulin content of each pellet and the mean microtubule length (Materials and Methods), we found that eribulin bound to microtubules in a concentration-dependent manner, as shown in Figure 3A and as a double-reciprocal plot in Figure 3B. At the lowest eribulin concentration (0.1 μM), an average of 0.48 eribulin molecule bound per microtubule. The stoichiometry increased to a value of 6.1 eribulins per microtubule at 2 μM, above which binding approached saturation, as indicated by a change in the slope of the curve. At 10 μM, binding was 11 eribulins per microtubule. Nonlinear regression analysis (Materials and Methods) indicated that eribulin binds to microtubules with a Y_{max} of 14.7 ± 1.3 eribulins per microtubule and a K_d of 3.5 ± 0.6 μM eribulin. The low binding maximum is indicative of binding to microtubule ends, where there is an average of 13 tubulin dimers exposed at each end (*25*).

Vinblastine Inhibits the Binding of < 5 μM Eribulin and Enhances the Binding of > 5 μM Eribulin to Microtubule Ends in Vitro. To study the eribulin binding site and its location relative to the vinca domain, we examined the influence of vinblastine on binding of eribulin to microtubules. Vinblastine (2 or 4 μM) was added to sheared, steady-state, MAP-rich microtubules for 15 min before addition of [^{3}H]eribulin (0.1−10 μM). Microtubule lengths were determined, and after centrifugation through a glycerol/DMSO cushion and determination

of tubulin mass and the amount of bound eribulin in the pellets, the number of eribulin molecules bound per microtubule was calculated (Figure 4A).

The results for the low eribulin concentration range (0.1−2 μM) are shown enlarged in Figure 4B. Vinblastine inhibited eribulin binding at low eribulin concentrations, consistent with previous findings with soluble tubulin (*2*, *10*). At the lowest eribulin concentration, vinblastine (2 μM) inhibited binding of eribulin (0.1 μM) to microtubules by 44% (from 0.48 ± 0.06 to 0.27 ± 0.05 eribulin molecule per microtubule ± SEM). Surprisingly, the extent of inhibition decreased as the eribulin concentration was increased; 2 μM vinblastine inhibited 5 μM eribulin slightly, but the change in eribulin per microtubule was not significant (from 8.7 ± 1.1 to 8.1 ± 0.72). At 10 μM eribulin, 2 μM vinblastine strengthened eribulin binding by 36% (from 11 ± 1.2 to 15 ± 1.1). These unique effects were further enhanced at 4 μM vinblastine: the level of binding of 0.1 μM eribulin was reduced by 63% (from 0.48 ± 0.06 to 0.18 ± 0.004), the level of binding of 5 μM eribulin was reduced only slightly and not significantly (from 8.7 ± 1.1 to 7.8 ± 0.33), and the level of binding of 10 μM eribulin was increased by 55% (from 11 ± 1.2 to 17 ± 1.7).

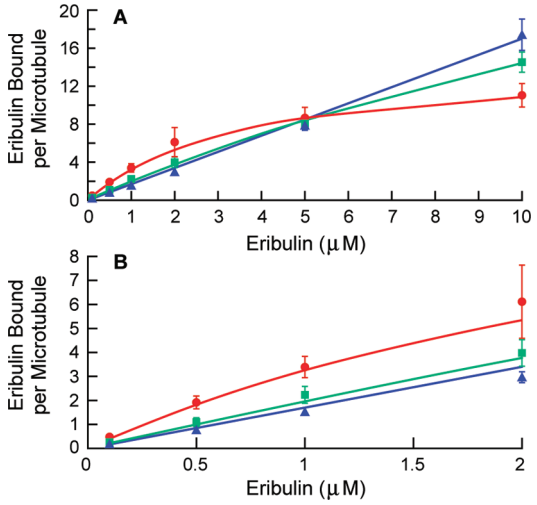

FIGURE 4: Effects of vinblastine on binding of eribulin to microtubules. (A) Vinblastine inhibited eribulin binding at low eribulin concentrations but strengthened binding at high eribulin concentrations. (B) Enlargement of panel A showing effects of vinblastine at low eribulin concentrations. Vinblastine was added to microtubules and incubated for 15 min before [^{3}H]eribulin was added. Eribulin binding in the absence of vinblastine (red circles) and in the presence of 2 μM vinblastine (green squares) and 4 μM vinblastine (blue triangles). Nonlinear regression (Materials and Methods) was used to generate the curves for control and 2 μM vinblastine; a simple linear equation was used for 4 μM vinblastine.

The Effects of Eribulin on Microtubule Structure Differ from Those of Vinblastine. Microtubule ends after incubation of MAP-rich microtubules with 50 μM eribulin or 50 μM vinblastine are shown in Figure 5. The ends of the control and eribulin-treated microtubules were blunt or slightly splayed; however, no extensively splayed or spiraled protofilaments occurred (Figure 5A,B). In contrast, all of the vinblastine-treated microtubules had extremely splayed ends, many with long, spiraled protofilaments emanating from one or both ends (Figure 5C). The structures of the microtubule ends were examined for control, eribulin-treated, and vinblastine-treated microtubules (Table 2). Fifty microtubules were counted for control and eribulin-treated microtubules, and 30 microtubules were counted for vinblastine-treated microtubules. The majority (72%) of control microtubules showed no splaying at either end, compared with 34% of eribulin-treated microtubules. A single end was slightly splayed in 44% of eribulin-treated microtubules, and 22% had both ends slightly splayed, compared with 24% and 4% of control microtubules, respectively. In contrast, all of the vinblastine-treated microtubules were splayed or spiraled at both

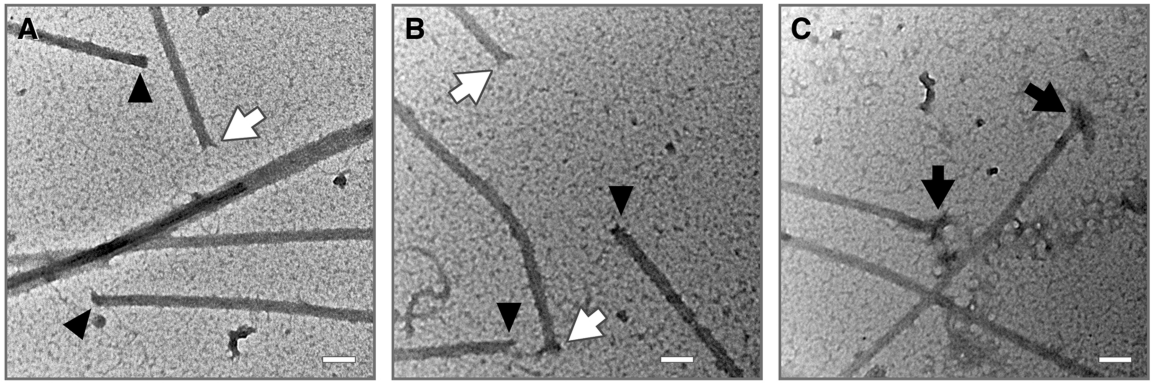

FIGURE 5: Electron micrographs of microtubules after incubation with (A) no drug, (B) 50 μM eribulin, or (C) 50 μM vinblastine. Ends in controls or eribulin-treated microtubules were either blunt (black triangles) or splayed (white arrows). After incubation with vinblastine, all ends were extensively splayed and many had protruding spiraled protofilaments (black arrows). Magnification of 100000× and scale bar of 100 nm.

Table 2: Structures of Microtubule Ends in the Absence of Drug or in the Presence of 50 μM Eribulin or 50 μM Vinblastine

	control[a]	eribulin, 50 μM	vinblastine, 50 μM
both ends blunted	72%	34%	
one end slightly splayed, one end blunted	24%	44%	
both ends slightly splayed	4%	22%	
one end slightly splayed, one end extensively splayed or spiraled			20%
both ends extensively splayed or spiraled			80%

[a]Fifty microtubules were examined for control and eribulin-treated microtubules, and 30 microtubules were examined for vinblastine-treated microtubules.

ends and most of them (80%) were extensively splayed or spiraled at both ends, whereas none of the eribulin-treated microtubules exhibited this morphology at either end.

DISCUSSION

We found that eribulin binds to a single site on soluble tubulin with a low affinity and to a very small number of sites at microtubule ends with a high affinity. The binding to soluble tubulin is complex with an intermediate plateau occurring at $\leq 10\ \mu$M eribulin with a stoichiometry of 0.26 ± 0.02 eribulin per tubulin dimer with an apparent very high affinity ($K_d = 0.4 \pm 0.2\ \mu$M) (discussed further below). At higher eribulin concentrations, the drug bound 1.3 ± 0.4 saturable low-affinity sites per tubulin dimer ($K_d = 46 \pm 28\ \mu$M). Eribulin bound with high affinity ($K_d = 3.5 \pm 0.6\ \mu$M) to 14.7 ± 1.3 saturable sites per microtubule, indicating high-affinity binding to microtubule ends. Eribulin had no significant effect on dynamic instability at microtubule minus ends in contrast to its potent suppression of growth rates and lengths at plus ends. When added to steady-state MAP-rich microtubules, eribulin induced an immediate transient depolymerization proportional to the eribulin concentration, before attaining a new steady-state polymer mass. In the presence of vinblastine, eribulin binding to microtubules was inhibited at $\leq 5\ \mu$M eribulin, but above 5 μM, eribulin binding was strengthened.

The reason for the complex nature of the binding to soluble tubulin (Figure 1B) is not clear. We found that a plateau in the binding occurred between 1 and 10 μM eribulin with only ~25% of the tubulin bound. At concentrations above 10 μM, eribulin bound the remainder of the tubulin, with complete saturation at a ratio of eribulin to tubulin slightly higher than 1:1. There are at least three conceivable explanations for the intermediate plateau in the binding isotherm. One explanation might be differing affinities of eribulin for binding to different tubulin isotypes. Bovine brain tubulin contains a mixture of several tubulin isotypes, of which $\alpha\beta_{III}$ tubulin is approximately 25% of the total (*27*) and is therefore a candidate for such putative high-affinity eribulin binding. It is also formally conceivable that there are two eribulin binding sites on the β_{III} tubulin molecule, one of high affinity and the second of lower affinity thus yielding a maximal overall stoichiometry of 1.3 eribulin molecules per tubulin, although we consider this unlikely. The third possibility is that the plateau in the binding isotherm is artifactual. Tubulin tends to self-associate and form oligomers, and this is largely inhibited by eribulin (*28*). Since eribulin does not appear to bind with significant affinity to the sides of microtubules, it is conceivable that at lower eribulin concentrations ($\leq 10\ \mu$M), tubulin oligomerization competes for the eribulin binding site, causing an artifactual plateau in the isotherm, a phenomenon that would be negated at higher eribulin concentrations. To discern among the potential causes will require further experimentation.

The addition of eribulin to MAP-rich microtubules induced a rapid transient depolymerization before a new reduced steady-state polymer mass was attained (Figure 2A). Half-maximal depolymerization of microtubules occurred at 11 μM eribulin; at this concentration, 11 eribulin molecules were bound per microtubule. The extent of depolymerization after 30 min (Figure 2B) was directly proportional to the eribulin concentration, suggesting that a depletion of the soluble tubulin pool by binding to eribulin is directly responsible for the decrease in polymer mass. The concentration of microtubule ends was approximately 5 nM, while the soluble tubulin concentration was much higher, equaling approximately 40% of the total tubulin concentration in the control, or ~8 μM. Therefore, although the K_d for binding of eribulin to soluble tubulin is more than 10-fold higher than for tubulin in microtubules, the concentration of soluble tubulin is more than 1000 times higher than the concentration of microtubules end, resulting in a significant portion of eribulin binding to soluble tubulin as well as to microtubule ends.

The depolymerization may at first appear contradictory to our previous finding that, at steady state, low concentrations of eribulin (100 nM) suppressed the growth rate of microtubule dynamic instability but had no significant effect on the shortening rate (*11*). However, in explanation, when eribulin is added to microtubules, it binds to tubulin in the soluble pool, reducing the amount of free soluble tubulin available to add to the microtubule ends and thus upsetting the steady-state equilibrium between dynamic microtubules and soluble tubulin. Sufficient tubulin must then be lost from the microtubules by depolymerization to re-establish a new steady state.

Eribulin bound a maximum of 15 sites per microtubule (Figure 3). Saturation at such a low number of drug molecules per microtubule strongly indicates binding at microtubule ends. Microtubules contain a small number of exposed tubulin dimers at each end, between 12 and 14 per end, versus nearly 2000 potential binding sites per micrometer of length along the microtubule lattice (*25*). These data suggest that eribulin binds to only one end of a microtubule, since binding to both ends would likely result in a higher binding maximum. These binding sites in microtubules had a high affinity for eribulin, more than 10 times higher than the affinity of eribulin for binding to soluble tubulin, suggesting that the primary mechanism of eribulin is to bind to microtubule ends to exert its effect.

Eribulin potently inhibited microtubule plus end growth by 46−50% (Table 1 and ref *11*) when only 0.5 eribulin molecule was bound per microtubule [at 100 nM eribulin (Figure 3)]. Thus, the binding of a single eribulin molecule at the end of a microtubule can strongly inhibit microtubule growth. It is likely that the binding of eribulin or an eribulin−tubulin complex to a microtubule end may sterically hinder the addition of new tubulin dimers to growing protofilaments.

At 100 nM eribulin, there was no significant change in microtubule dynamic instability at minus ends (Table 1). The evidence indicating that eribulin preferentially suppresses plus end dynamic instability, and that eribulin binds to a maximum of 15 sites per microtubule, strongly suggests that eribulin binds primarily at the plus ends of microtubules. These data, together with the result that eribulin binds $\alpha-\beta$ tubulin heterodimers at a single site (Figure 1C), suggest that the β-tubulin subunit contains the major portion of the eribulin binding site. These data are in agreement with recent results from Alday and Correia (*28*) suggesting that eribulin does not bind to both α- and β-tubulin but binds to either the interdimer interface or the β-tubulin subunit alone.

By electron microscopy, we showed that eribulin at a high concentration (50 μM) did not induce extensive protofilament spiraling at microtubule ends which occurs with vinblastine (Figure 5). The ends of the microtubules were blunt or slightly splayed (Table 2). This finding supports the model in which eribulin binds β-tubulin with high affinity and α-tubulin with low or no affinity, and thus, eribulin does not "link" tubulin heterodimers together in the manner of vinblastine, which binds both

subunits nearly equally (*17*). However, the presence of the slightly splayed microtubule ends suggests a possible low-affinity binding to α-tubulin. Since 22% of eribulin-treated microtubules exhibited slight splaying at both ends, it appears that at sufficiently high concentrations, eribulin may bind minus ends.

Vinblastine inhibited binding of eribulin to microtubules at low eribulin concentrations (≤5 μM) (Figure 4A,B). Unexpectedly, vinblastine induced an increase in the number of eribulin binding sites per microtubule at higher eribulin concentrations, increasing from 11 to 14 and 17 eribulin molecules per microtubule in the presence of 2 and 4 μM vinblastine, respectively (Figure 4A). This slight increase in the level of binding suggests that the vinblastine-induced splaying of protofilaments allows increased access of eribulin to additional sites at the microtubule end (*29*).

ACKNOWLEDGMENT

We thank Mr. Herb Miller for expert purification of bovine brain tubulin and Dr. John Lew and Dr. John Correia for valuable discussions of the binding analysis.

REFERENCES

1. Towle, M. J., Salvato, K. A., Budrow, J., Wels, B. F., Kuznetsov, G., Aalfs, K. K., Welsh, S., Zheng, W., Seletsk, B. M., Palme, M. H., Habgood, G. J., Singer, L. A., Dipietro, L. V., Wang, Y., Chen, J. J., Quincy, D. A., Davis, A., Yoshimatsu, K., Kishi, Y., Yu, M. J., and Littlefield, B. A. (2001) In vitro and in vivo anticancer activities of synthetic macrocyclic ketone analogues of halichondrin B. *Cancer Res. 61*, 1013–1021.
2. Dabydeen, D. A., Burnett, J. C., Bai, R. L., Verdier-Pinard, P., Hickford, S. J. H., Pettit, G. R., Blunt, J. W., Munro, M. H. G., Gussio, R., and Hamel, E. (2006) Comparison of the activities of the truncated halichondrin B analog NSC 707389 (E7389) with those of the parent compound and a proposed binding site on tubulin. *Mol. Pharmacol. 70*, 1866–1875.
3. Hirata, Y., and Uemura, D. (1986) Halichondrins: Antitumor Polyether Macrolides from a Marine Sponge. *Pure Appl. Chem. 58*, 701–710.
4. Goel, S., Mita, A. C., Mita, M., Rowinsky, E. K., Chu, Q. S., Wong, N., Desjardins, C., Fang, F., Jansen, M., Shuster, D. E., Mani, S., and Takimoto, C. H. (2009) A Phase I Study of Eribulin Mesylate (E7389), a Mechanistically Novel Inhibitor of Microtubule Dynamics, in Patients with Advanced Solid Malignancies. *Clin. Cancer Res. 15*, 4207–4212.
5. Tan, A. R., Rubin, E. H., Walton, D. C., Shuster, D. E., Wong, Y. N., Fang, F., Ashworth, S., and Rosen, L. S. (2009) Phase I study of eribulin mesylate administered once every 21 days in patients with advanced solid tumors. *Clin. Cancer Res. 15*, 4213–4219.
6. Vahdat, L. T., Pruitt, B., Fabian, C. J., Rivera, R. R., Smith, D. A., Tan-Chiu, E., Wright, J., Tan, A. R., DaCosta, N. A., Chuang, E., Smith, J., O'Shaughnessy, J., Shuster, D. E., Meneses, N. L., Chandrawansa, K., Fang, F., Cole, P. E., Ashworth, S., and Blum, J. L. (2009) Phase II Study of Eribulin Mesylate, a Halichondrin B Analog, in Patients With Metastatic Breast Cancer Previously Treated With an Anthracycline and a Taxane. *J. Clin. Oncol. 27*, 2954–2961.
7. Postma, T. J., Vermorken, J. B., Liefting, A. J., Pinedo, H. M., and Heimans, J. J. (1995) Paclitaxel-induced neuropathy. *Ann. Oncol. 6*, 489–494.
8. Pace, A., Bove, L., Nistico, C., Ranuzzi, M., Innocenti, P., Pietrangeli, A., Terzoli, E., and Jandolo, B. (1996) Vinorelbine neurotoxicity: Clinical and neurophysiological findings in 23 patients. *J. Neurol. Neurosurg. Psychiatry 61*, 409–411.
9. Quasthoff, S., and Hartung, H. P. (2002) Chemotherapy-induced peripheral neuropathy. *J. Neurol. 249*, 9–17.
10. Bai, R., Paull, K. D., Herald, C. L., Malspeis, L., Pettit, G. R., and Hamel, E. (1991) Halichondrin-B and Homohalichondrin-B, Marine Natural-Products Binding in the Vinca Domain of Tubulin: Discovery of Tubulin-Based Mechanism of Action by Analysis of Differential Cytotoxicity Data. *J. Biol. Chem. 266*, 15882–15889.
11. Jordan, M. A., Kamath, K., Manna, T., Okouneva, T., Miller, H. P., Davis, C., Littlefield, B. A., and Wilson, L. (2005) The primary antimitotic mechanism of action of the synthetic halichondrin E7389 is suppression of microtubule growth. *Mol. Cancer Ther. 4*, 1086–1095.
12. Okouneva, T., Azarenko, O., Wilson, L., Littlefield, B. A., and Jordan, M. A. (2008) Inhibition of centromere dynamics by eribulin (E7389) during mitotic metaphase. *Mol. Cancer Ther. 7*, 2003–2011.
13. Jordan, M. A., and Kamath, K. (2007) How do microtubule-targeted drugs work? An overview. *Curr. Cancer Drug Targets 7*, 730–742.
14. Jordan, M. A., and Wilson, L. (2004) Microtubules as a target for anticancer drugs. *Nat. Rev. Cancer 4*, 253–265.
15. Cormier, A., Marchand, M., Ravelli, R. B. G., Knossow, M., and Gigant, B. (2008) Structural insight into the inhibition of tubulin by vinca domain peptide ligands. *EMBO Rep. 9*, 1101–1106.
16. Hamel, E. (1992) Natural Products Which Interact with Tubulin in the Vinca Domain: Maytansine, Rhizoxin, Phomopsin-a, Dolastatin-10 and Dolastatin-15 and Halichondrin-B. *Pharmacol. Ther. 55*, 31–51.
17. Gigant, B., Wang, C., Ravelli, R. B., Roussi, F., Steinmetz, M. O., Curmi, P. A., Sobel, A., and Knossow, M. (2005) Structural basis for the regulation of tubulin by vinblastine. *Nature 435*, 519–522.
18. Littlefield, B. A., Palme, M., Seletsky, B. M., Towle, M. J., Melvin, Y. J., and Zheng, W. (2001) Macrocyclic analogs and methods of their use and preparation, Eisai Co. Ltd., Andover, MA.
19. Toso, R. J., Jordan, M. A., Farrell, K. W., Matsumoto, B., and Wilson, L. (1993) Kinetic stabilization of microtubule dynamic instability in vitro by vinblastine. *Biochemistry 32*, 1285–1293.
20. Bradford, M. M. (1976) A rapid and sensitive method for the quantitation of microgram quantities of protein utilizing the principle of protein-dye binding. *Anal. Biochem. 72*, 248–254.
21. Panda, D., Goode, B. L., Feinstein, S. C., and Wilson, L. (1995) Kinetic stabilization of microtubule dynamics at steady state by tau and microtubule-binding domains of tau. *Biochemistry 34*, 11117–11127.
22. Walker, R. A., O'Brien, E. T., Pryer, N. K., Soboeiro, M. F., Voter, W. A., Erickson, H. P., and Salmon, E. D. (1988) Dynamic instability of individual microtubules analyzed by video light microscopy: Rate constants and transition frequencies. *J. Cell Biol. 107*, 1437–1448.
23. Derry, W. B., Wilson, L., and Jordan, M. A. (1998) Low potency of taxol at microtubule minus ends: Implications for its antimitotic and therapeutic mechanism. *Cancer Res. 58*, 1177–1184.
24. Loike, J. D., Brewer, C. F., Sternlicht, H., Gensler, W. J., and Horwitz, S. B. (1978) Structure-activity study of the inhibition of microtubule assembly in vitro by podophyllotoxin and its congeners. *Cancer Res. 38*, 2688–2693.
25. Amos, L., and Klug, A. (1974) Arrangement of subunits in flagellar microtubules. *J. Cell Sci. 14*, 523–549.
26. Jordan, M. A., and Wilson, L. (1990) Kinetic analysis of tubulin exchange at microtubule ends at low vinblastine concentrations. *Biochemistry 29*, 2730–2739.
27. Banerjee, A., Roach, M. C., Wall, K. A., Lopata, M. A., Cleveland, D. W., and Luduena, R. F. (1988) A monoclonal antibody against the type II isotype of β-tubulin. Preparation of isotypically altered tubulin. *J. Biol. Chem. 263*, 3029–3034.
28. Alday, P. H., and Correia, J. J. (2009) Macromolecular Interaction of Halichondrin B Analogues Eribulin (E7389) and ER-076349 with Tubulin by Analytical Ultracentrifugation. *Biochemistry 48*, 7927–7938.
29. Wilson, L., Jordan, M. A., Morse, A., and Margolis, R. L. (1982) Interaction of vinblastine with steady-state microtubules in vitro. *J. Mol. Biol. 159*, 125–149.